



Effect of Varying H₂S Content on High-Temperature Corrosion of Ferritic and Austenitic Alloys in a Simulated Pyrolysis Process of Post-Consumer Plastics

Manuela Nimmervoll¹, Gregor Mori¹, Edith Bucher¹, Stefan Hönig², and Roland Haubner³

¹Montanuniversität Leoben, Leoben, Austria

²OMV E&P GmbH, Gänserndorf, Austria

³Technische Universität Wien, Vienna, Austria

Received May 4, 2021; accepted May 25, 2021; published online June 29, 2021

Abstract: The alloys K90941 and N08811 were tested under conditions simulating a pyrolysis process of post-consumer plastics. Impurities in the plastic feedstock like chlorine containing materials or organic components yield HCl and H₂S respectively during the cracking process. The reactor material must be able to withstand these harsh corrosive conditions.

In lab-scale test equipment, process conditions of the reactor zone of the pyrolysis process were simulated at temperatures of 420 °C and 580 °C for 72 h. The gas atmosphere consisted of either 200 ppm or 20000 ppm H₂S and 3.8 vol% HCl, 1.9 vol% CO₂, 0.3 vol% CO, 2.8 vol% H₂, bal. N₂. After the corrosion experiments, the samples were analyzed by metallography, SEM/EDX, and XRD. Additionally, the mass loss was evaluated. Results show that the ferritic K90941 is more aggressively attacked than the austenitic N08811 and that for both materials the mass loss rises with increasing H₂S content in the gas atmosphere and increasing temperature.

Keywords: High temperature corrosion, Hydrogen chloride, Hydrogen sulfide, Stainless steel

Einfluss des variablen H₂S Gehalts auf die Hochtemperaturkorrosion ferritischer und austenitischer Legierungen in einem simulierten Pyrolyseprozess von Post-Consumer Plastik

Zusammenfassung: Die Legierungen K90941 und N08811 wurden unter simulierten Bedingungen eines Pyrolyseprozesses von Post-Consumer Plastik getestet. Verunreinigungen

im Plastik-Einsatzmaterial, wie z. B. chlorhaltige Materialien oder organische Komponenten, können während des Crackingprozesses zur Bildung von HCl und H₂S führen. Das Reaktormaterial muss diesen stark korrosiven Bedingungen standhalten.

In einer Versuchsanlage im Labormaßstab wurden die Prozessbedingungen der Reaktorzone eines Pyrolyseprozesses bei 420 °C und 580 °C für 72 h simuliert. Die Gasatmosphäre bestand aus entweder 200 ppm oder 20000 ppm H₂S und je 3,8 vol% HCl, 1,9 vol% CO₂, 0,3 vol% CO, 2,8 vol% H₂, bal. N₂. Nach den Korrosionsexperimenten wurden die Proben mittels Metallographie, SEM/EDX und XRD analysiert. Zusätzlich wurde der Masseverlust bestimmt. Die Ergebnisse zeigen, dass das ferritische Material, K90941, stärker attackiert wird als das austenitische Material, N08811. Außerdem steigt der Masseverlust für beide Materialien mit steigendem H₂S Gehalt in der Gasatmosphäre und steigender Temperatur an.

Schlüsselwörter: Hochtemperaturkorrosion, Chlorwasserstoff, Schwefelwasserstoff, Rostfreier Stahl

1. Introduction

Thermal cracking of anthropogenic resources, like post-consumer plastics, is a promising chemical recycling route and a good alternative to disposal. Still, thermal cracking is a demanding process for metallic materials, since impurities in the post-consumer plastics, like chlorine containing materials or biological components, yield HCl and H₂S respectively during cracking. These two gas components are known to cause high temperature corrosion and, thus, lead to damage of metallic materials [1–4].

In other industrial processes, construction materials also suffer from chlorine and/or sulfur induced high temperature corrosion, e.g. ethyldichloride production or gasification

Dipl.-Ing. M. Nimmervoll (✉)
Montanuniversität Leoben,
Franz Josef Straße 18,
8700 Leoben, Austria
manuela.nimmervoll@unileoben.ac.at

of biomass. Alloys which can form protective scales in atmospheres with high partial pressures of oxygen are often not able to do so in atmospheres that contain chlorine [5]. The reason for this is that HCl gas or chlorine penetrate the metals initial oxide layer and form volatile metal chlorides underneath this protective layer with the base material. At temperatures above 400°C, these metal chlorides are volatile and evaporate causing a subsequent outward diffusion through the initial oxide scale until they reach the interface to the gas atmosphere. There the oxygen pressure is high enough to oxidize the metal chlorides, which results in the formation of loose and non-protective oxide layers. This type of corrosion is also known as "active corrosion". Fortunately, some research has already been done on gas atmospheres with chlorine and sulfur simultaneously present [1, 6–12].

Yet, investigations about the corrosion of steels at low oxygen partial pressure and in the presence of chlorine and sulfur are rare [2, 13]. Only a few authors have dealt with this topic and even found differing results in some cases. Pan et al. [14] reported that the corrosion rates of Fe-Cr alloys in a mixed H₂-HCl-CO₂ atmosphere accelerated with an increasing H₂S level. Bakker and Perkins [15, 16] also reported an increase of corrosion rates of Fe in mixtures of H₂S and HCl above 400°C but a decrease in sulfidation below 399°C. Other authors found a reduction of corrosion rates by the addition of H₂S in chlorine containing atmospheres [11]. Thus, the high temperature corrosion behavior of metals in these complex gas atmospheres requires further investigation.

To assess the applicability of a durable reactor material for a thermal cracking process of post-consumer plastics, the corrosion behavior of two commonly used construction materials was investigated. Therefore, the ferritic steel K90941 and the austenitic steel N08811 were tested under conditions simulating the thermal cracking process for 72 h followed by comparing the different results.

2. Experimental Procedure

The corrosion behavior of ferritic steel K90941 and austenitic steel N08811 was tested under conditions simulating a pyrolysis process of post-consumer plastics. The high-temperature corrosion tests were performed at laboratory scale in a heated silica glass tube at 420°C and 580°C for 72 h. The selection of the testing temperatures was based on the knowledge gained in a pilot plant. The corrosive test gas atmosphere consisted of either 200 ppm or 20000 ppm H₂S and 3.8 vol% HCl, 1.9 vol% CO₂, 0.3 vol% CO, 2.8 vol% H₂, bal. N₂. This atmosphere represented the partial pressures of sulfur, chlorine, and oxygen, which are present in the reactor zone of the pyrolysis process. The software FactSage 7.0 and PetroSIM were used to calculate the composition of the artificial gas mixture.

The gas mixture was provided in two separated bottles by Linde Gas (Eggendorf, AUT) as HCl cannot be stored together with H₂S. Stainless steel tubes were used to transport the gas from the bottles to the silica tube. During heating and cooling, the chamber was flushed with nitrogen.

TABLE 1
Chemical composition of the tested materials in wt% (balance Fe)

Material	C	Si	Mn	Cr	Mo	Ni
K90941	0.1	0.5	0.5	9	1	–
N08811	0.07	–	0.6	20.5	–	30.4

The test gas leaving the test chamber was neutralized in 10% KOH and 10% NaOH solution. A detailed experimental procedure and a scheme of the testing equipment can be found elsewhere [17].

Table 1 shows the chemical composition of the tested alloys. Before the corrosion tests were performed, all test specimens, which had a rectangular shape with dimensions of 25×10×2 mm, were metallographically polished up to 1000 grit SiC paper in order to achieve a uniform surface, cleaned, degreased, and gauged. For the corrosion experiments, four specimens of one material were accommodated simultaneously in the silica tube by using a silica glass holder. While three samples were used for the mass loss determination, one was cold mounted in epoxy resin for a metallographic and SEM/EDX investigation.

For the evaluation of the mass loss, the samples were cleaned with 5% hydrochloric acid and a wire brush. The removed corrosion products were characterized by XRD. Additionally, uncleaned samples were cold mounted in epoxy resin and polished up to 4000 μm SiC paper. The metallographic preparation of the corroded samples happened water-free to preserve water-soluble corrosion products for visualization of unaltered cross sections. The samples were investigated by means of light optical microscopy and SEM/EDX. SEM/EDX measurements were performed after 15 s gold sputtering, using a SEM by Zeiss (EVO MA 25 ®). The electron source was a LaB₆ cathode. Thermodynamic calculations were performed with the software Fact Sage 7.0.

3. Results

Fig. 1 shows the general appearance of the samples after the corrosion experiments. Both materials formed a loose and black layer of corrosion products under all conditions. The adhesion on the base metal and the thickness of this corrosion layer differed depending on material and temperature.

K90941, which was in general more aggressively attacked than N08811, had a thicker and less adherent layer of corrosion products. At a lower temperature, the adhesion of the corrosion layer improved for both materials with silver shiny dots being detected in between the corrosion layer. It is possible that these dots were iron chloride, since this phase was identified by XRD. Additionally, FeCl₂ was found at the colder parts of the silica tube (white crystals as shown in Fig. 1). The FeCl₂ formed at the samples, evaporated, was carried away with the gas flow, and then crystallized at the colder parts. The amount of FeCl₂ varied depending on the iron content of the alloy, the testing temperature, and the H₂S content in the atmosphere. The

Fig. 1: General appearance of the samples after the corrosion experiments

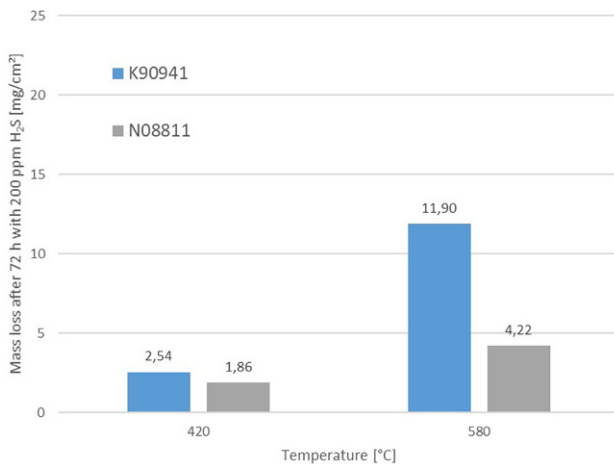
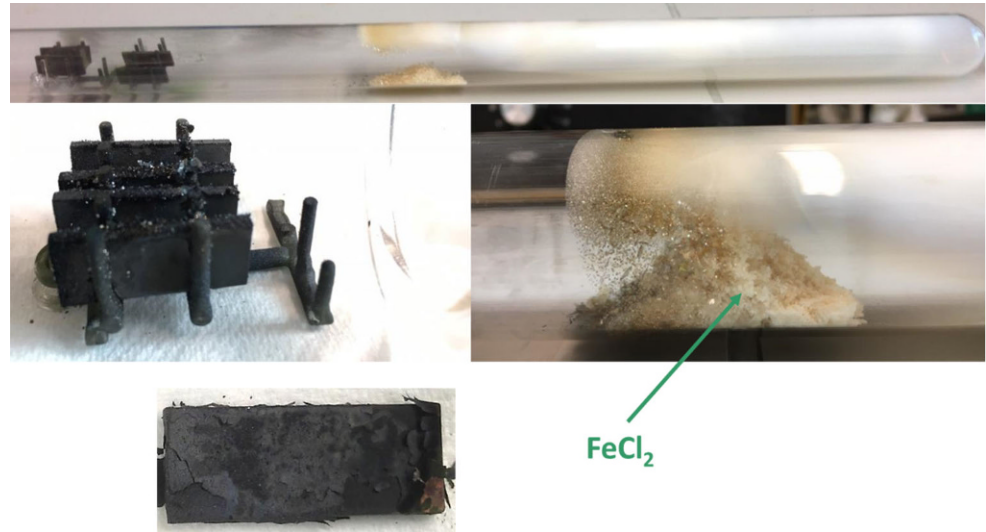


Fig. 2: Mass loss versus temperature of the tested materials after 72 h in the gas atmosphere containing 200 ppm H₂S

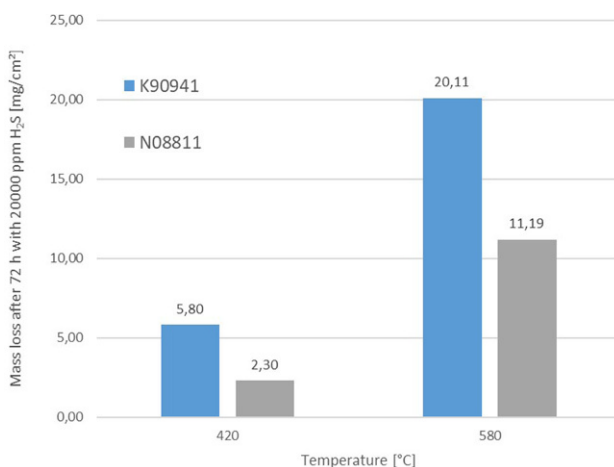


Fig. 3: Mass loss versus temperature of the tested materials after 72 h in the gas atmosphere containing 20000 ppm H₂S

amount of FeCl₂ increased with increasing iron content in the alloy, increasing temperature and decreasing H₂S content in the gas mixture. Both materials showed a uniform attack. In general, it is assumed that both materials are firstly attacked along the grain boundaries. Afterwards, successive metal removal of the grain occurs due to evaporating metal chlorides [18].

3.1 Corrosion Rates

Figs. 2 and 3 show the mass loss of the tested materials versus the temperature after 72 h in the gas atmosphere containing 200 ppm H₂S and 20000 ppm H₂S respectively. At 580 °C the ferritic K90941 shows a much higher mass loss than the austenitic N08811 in both atmospheres. At 420 °C and 200 ppm H₂S, the significant difference in mass loss between the materials disappeared and both alloys showed nearly the same corrosion rate. Still, the austenitic alloy performed slightly better than K90941. Moreover, the mass loss of N08811 did not increase drastically between 420 and 580 °C in the gas atmosphere containing 200 ppm H₂S, while K90941 mass loss more than quadrupled. As corrosion rates generally decrease with decreasing temperature because of slower reaction kinetics, the temperature dependence of the mass loss of the two materials were explainable. When going from 200 to 20000 ppm H₂S in the gas atmosphere, the mass loss of both materials increased. At 580 °C K90941 almost doubled its mass loss compared to the atmosphere with 200 ppm H₂S. N08811 even tripled its mass loss at 580 °C.

3.2 Corrosion Products

In order to get a better understanding of the corrosion behavior of the two alloys and to interpret the mass loss results, cross sections of the corroded samples were prepared by water-free polishing. The cross sections were later analyzed via SEM/EDX.

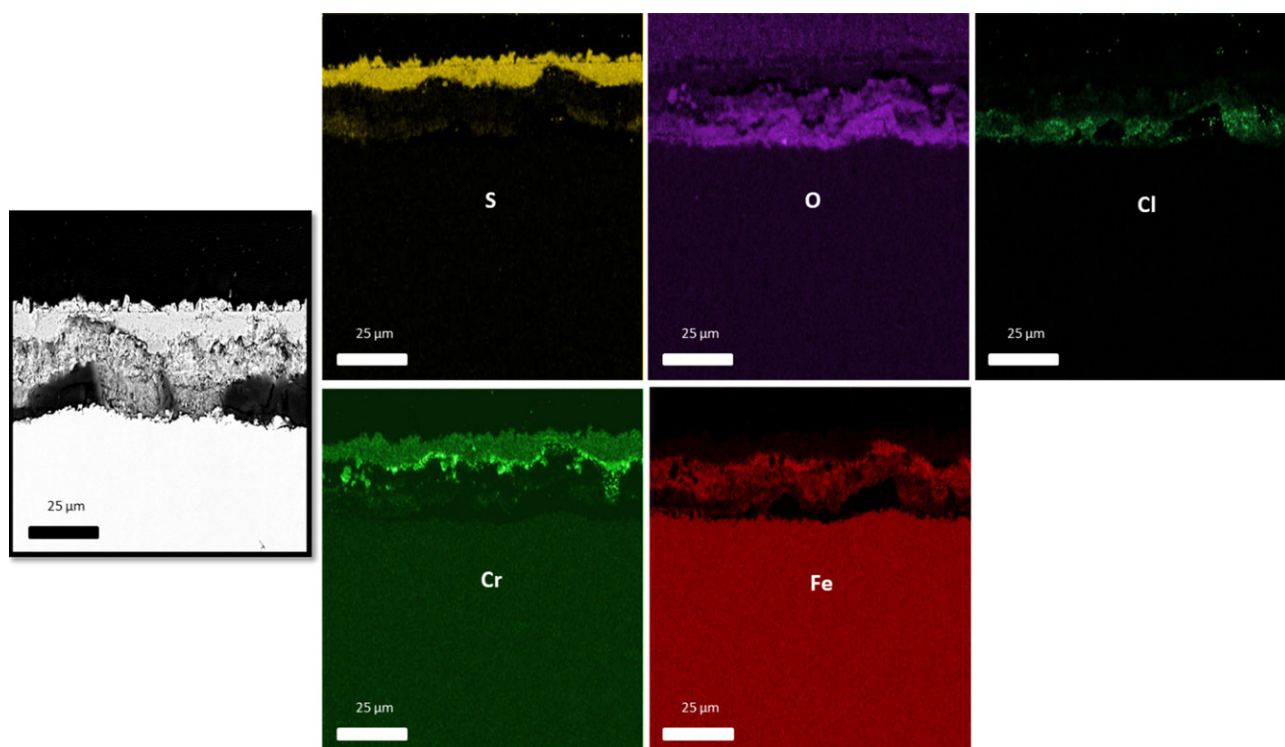


Fig. 4: Ferritic K90941 after 72 h, 200 ppm H₂S, 580 °C. SEM and EDX element mapping of the cross section

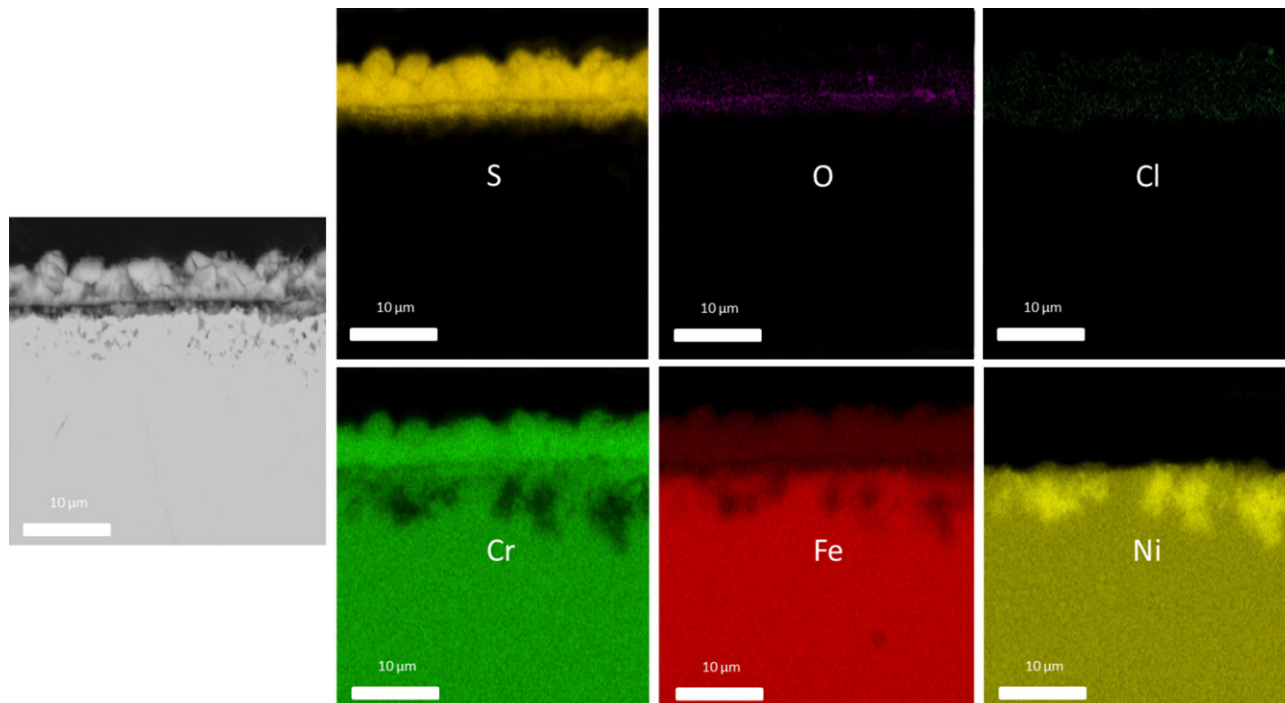


Fig. 5: Austenitic N08811 after 72 h, 200 ppm H₂S, 580 °C. SEM and EDX element mapping of the cross section

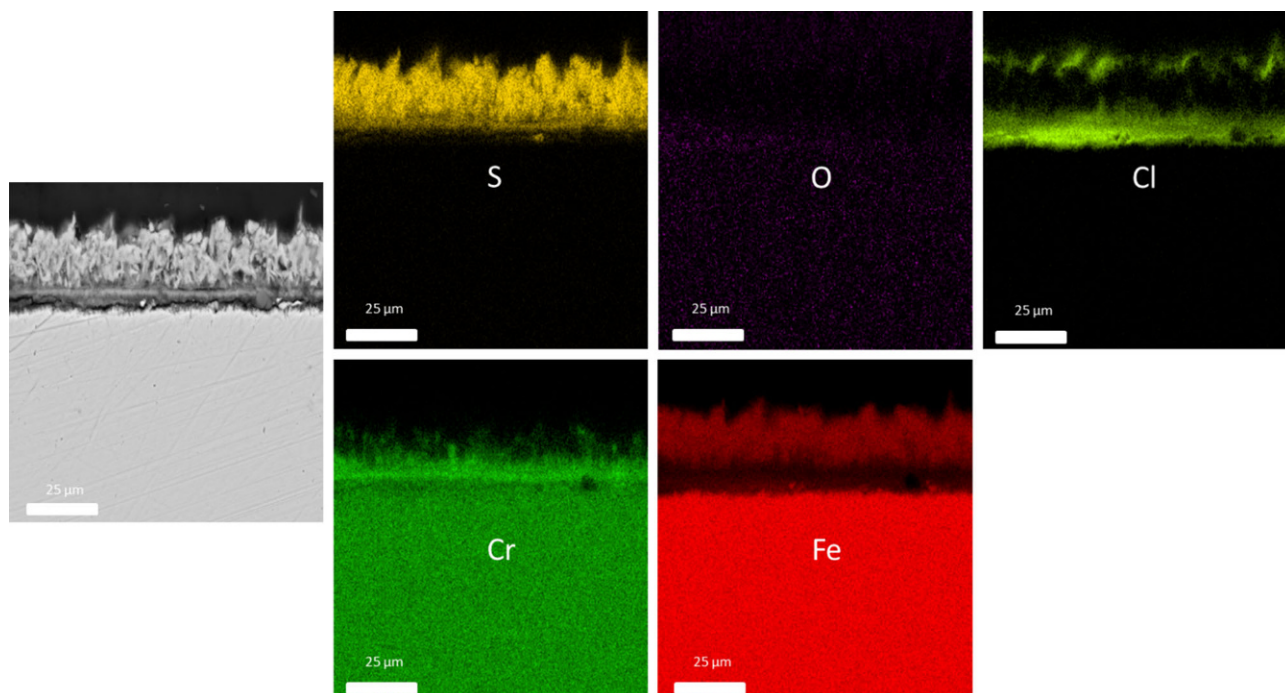


Fig. 6: Ferritic K90941 after 72 h, 200 ppm H₂S, 420 °C. SEM and EDX element mapping of the cross section

Figs. 4, 5, 6, 7, 8, 9, 10 and 11 illustrate the SEM images of the cross sections and the corresponding EDX mappings of the materials at the different conditions. In some of the SEM images a gap between the layer of corrosion products and the base metal can be seen. This reflects the bad adherence of the corrosion layer.

In Figs. 4 and 5, the corrosion behavior at 200 ppm H₂S at 580 °C can be seen for K90941 and N08811 respectively. Under these conditions, the picture of corrosion was different compared to all other conditions. In both materials, the EDX mapping detected a sulfide layer containing chromium in the outer regions of the corrosion products. The EDX mapping also revealed a small amount of iron inside the chromium sulfide layer. Yet, XRD of the corrosion products only detected Cr₂S₃ and Cr₃S₄.

Below the chromium sulfide layer an oxygen layer was observed, which was identified by XRD as Cr₂O₃. Beneath the oxygen layer and in between the sulfide layer, a certain amount of chlorine was detected. In the case of N08811 (Fig. 5), the EDX mapping showed a depletion of iron and chromium in the border area of the alloy, while nickel was enriched.

As mentioned above, iron and HCl formed volatile FeCl₂, which was found in the colder parts of the testing equipment. Chromium and HCl gas formed CrCl₂, which diffused through the corrosion layer and formed either oxide or sulfide, depending on the oxygen partial pressure. Nickel was not detected by XRD in any corrosion product. It remained metallic and showed no chemical reaction with the corresponding gas atmosphere at 580 °C. Thus, the detected chlorine can be explained by the formation of FeCl₂ and CrCl₂. As N08811 showed a smaller corrosive attack at

200 ppm H₂S and 580 °C than K90941, also the thickness of the corrosion layer was smaller.

As can be seen in Figs. 6 and 7, the corrosion behavior changed for both materials at 200 ppm H₂S at 420 °C. Again, both materials formed a sulfide layer on the surface. At 420 °C iron can be detected in the upper parts of the sulfide layer compared to 580 °C, where chromium was found on top. At lower temperatures chromium was only detected in the lower areas of the corrosion layer. XRD identified mixed sulfides of iron and chromium. In the case of N08811, nickel was detected in between the iron sulfide as well. XRD also identified several non-stoichiometric iron-nickel sulfides. The enrichment of nickel in the border area to the corrosion products could not be observed anymore. The presence of chlorine was not only restricted to the lower areas, but it was also detected on the surface of the corrosion layers. Furthermore, the amount of chlorine that could be detected in the corrosion products increased with decreasing temperature. This is because the vapor pressure of the metal chlorides decreases by lowering the temperature. Thus, less metal chlorides evaporated at 420 °C compared to 580 °C and therefore, remained on the samples. This was verified by XRD analysis, since FeCl₂ was detected in the corrosion products.

When going to higher H₂S contents of 20000 ppm in the gas phase, the corrosion behavior was similar to that at 200 ppm H₂S and 420 °C. At both temperatures, iron sulfide formed on the surface. Beneath the iron sulfide layer, a chromium containing layer was visible. In between the sulfide layer, also amounts of oxygen and chlorine could be detected. Compared to the atmosphere containing 200 ppm H₂S, the amount of the detected chlorine in the corrosion layer and as FeCl₂ at the colder parts of

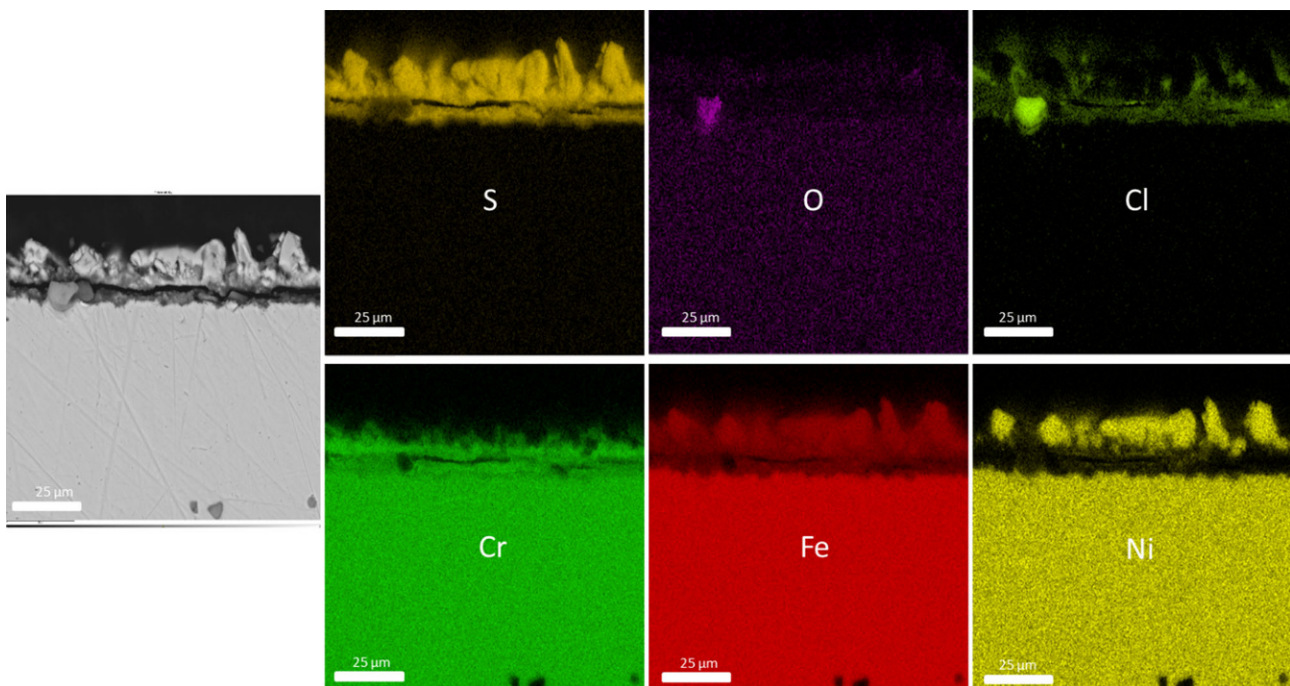


Fig. 7: Austenitic N08811 after 72 h, 200 ppm H₂S, 420 °C. SEM and EDX element mapping of the cross section

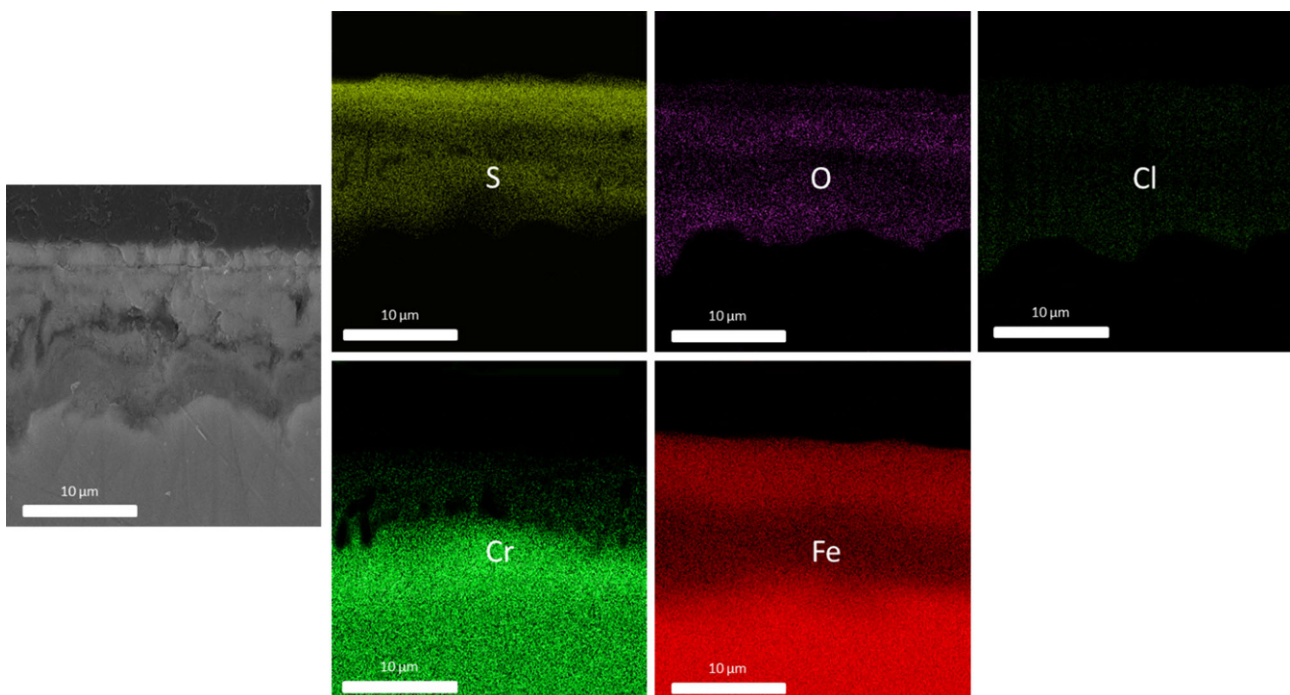


Fig. 8: Ferritic K90941 after 72 h, 20000 ppm H₂S, 580 °C. SEM and EDX element mapping of the cross section

the glass tube and oxygen decreased in the atmosphere with 20000 ppm H₂S. For N08811 also nickel was found in the upper iron sulfide layer, even for higher temperatures compared to low H₂S contents, where the nickel remains metallic. At 580 °C XRD only identified iron sulfide for K90941. XRD of the corrosion products of N08811 showed iron sulfide and a FeCr₂S₄ phase. K90941 with

less chromium than N08811 showed a thinner chromium containing layer than N08811.

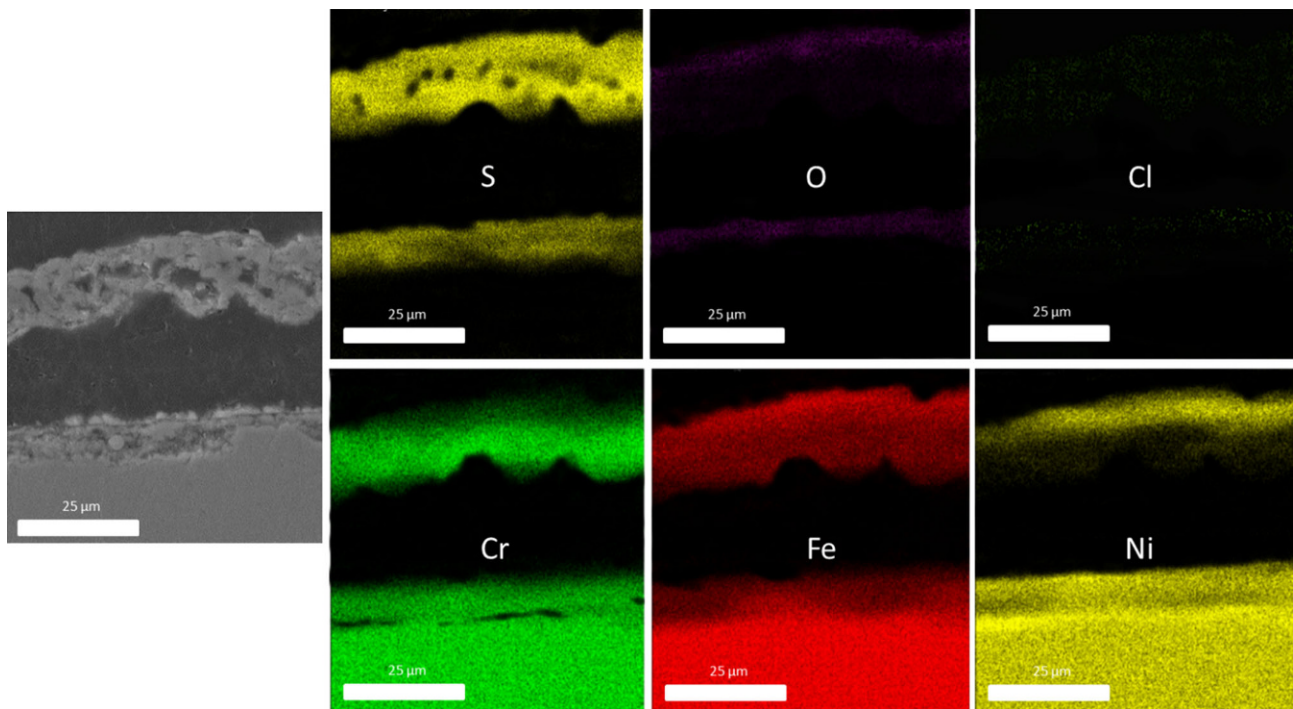


Fig. 9: Austenitic N08811 after 72 h, 20000 ppm H₂S, 580 °C. SEM and EDX element mapping of the cross section

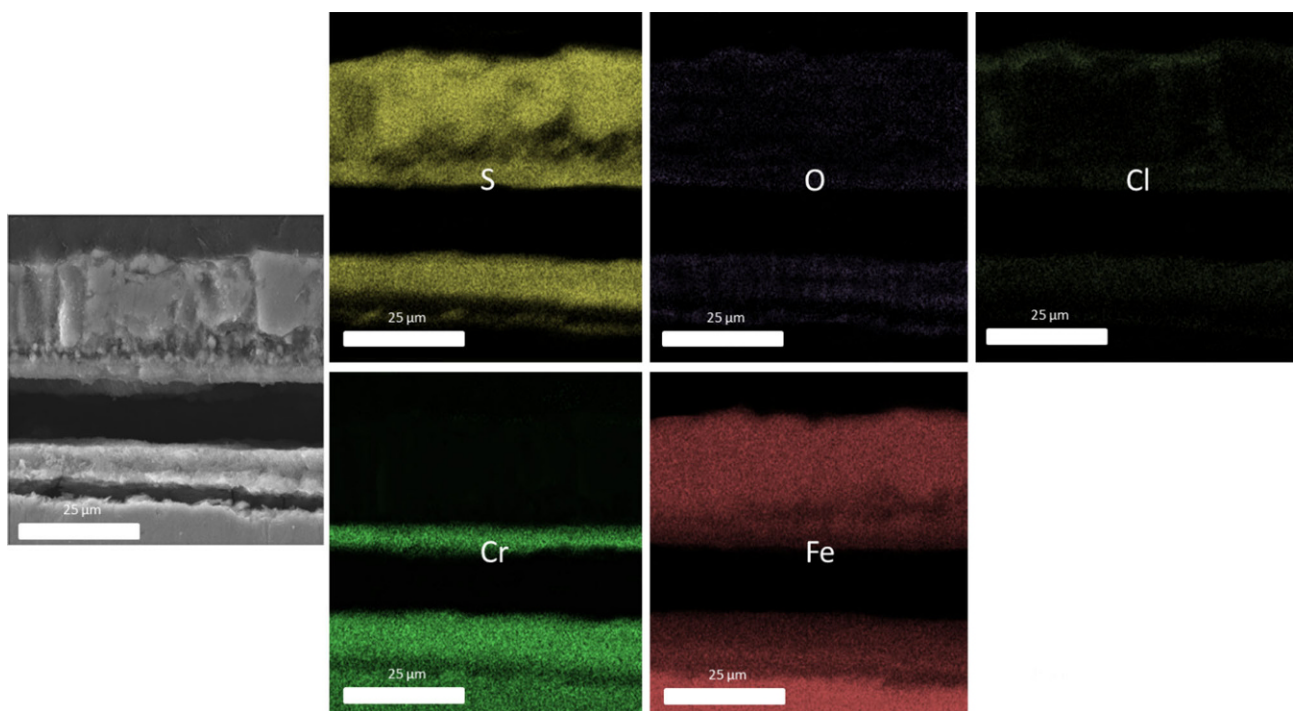


Fig. 10: Ferritic K90941 after 72 h, 20000 ppm H₂S, 420 °C. SEM and EDX element mapping of the cross section

3.3 Corrosion Mechanism

By interpretation of the XRD results and SEM/EDX mappings (Figs. 4, 5, 6, 7, 8, 9, 10 and 11) and by comparison with other research data, it is possible to give a rough explanation of the corrosion mechanisms.

At low H₂S amounts and at 580 °C, HCl is able to penetrate the initial oxide layer on the material and react with the base metal in order to form the corresponding metal chlorides. The Gibbs free energy of formation at 580 °C is negative for chromium and iron, and positive for nickel [17]. Thus, nickel remains metallic, while HCl is consumed

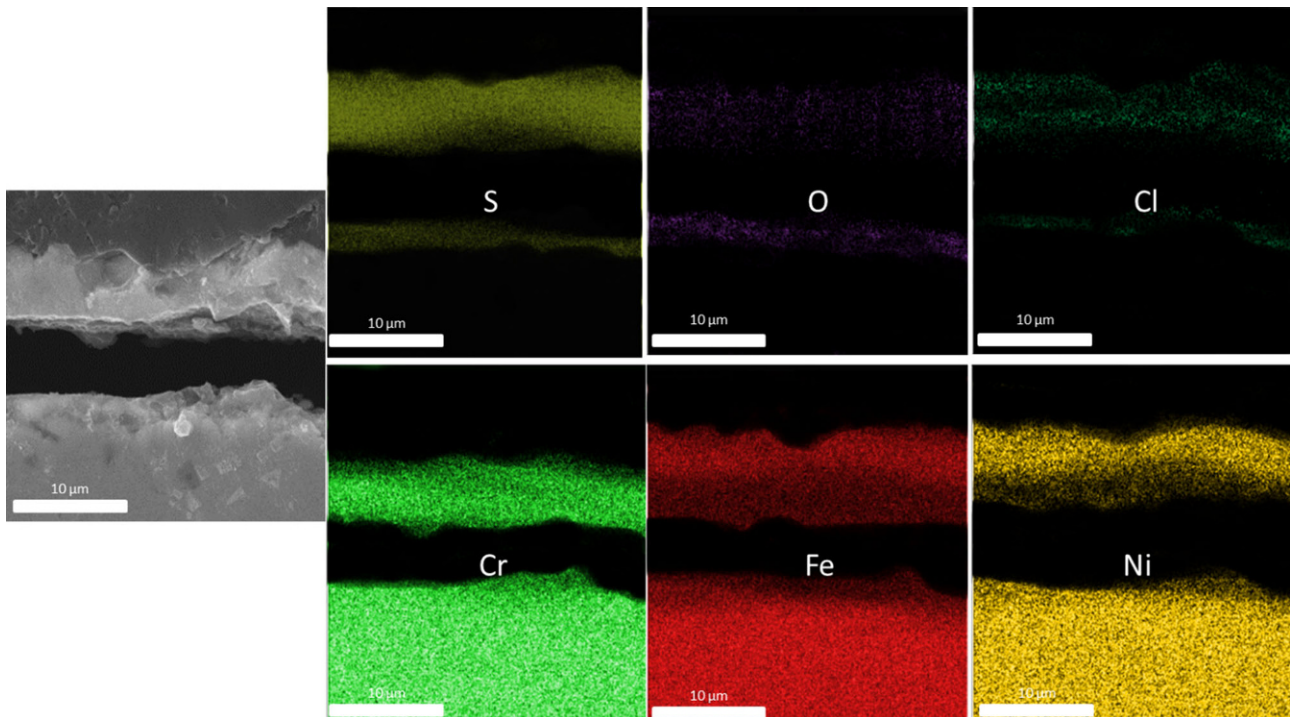
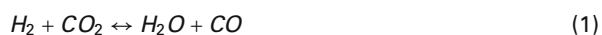


Fig. 11: Austenitic N08811 after 72h, 20000 ppm H₂S, 420°C. SEM and EDX element mapping of the cross section

by the formation of CrCl₂ and FeCl₂. The volatile metal chlorides evaporate because FeCl₂ has a higher vapor pressure. Thus, it evaporates faster and is partly carried away with the gas flow. This is the main reason for the weight loss of the samples during the experiments. Due to the water gas shift reaction, H₂O will be formed when CO₂ reacts with H₂ (see Eq. 1). This H₂O can react with CrCl₂ to form Cr₂O₃.



Excessive CrCl₂, which evaporates much more slowly compared to FeCl₂, diffuses out of the corrosion layer and reacts with H₂S at the surface to form mixed chromium sulfides. Thereby the findings of the EDX mappings and the XRD results can be explained. This mechanism has been identified in previous studies, and a detailed explanation can be found elsewhere [17].

At low H₂S amounts and at 420°C, the formation of mixed sulfides of iron and chromium and of iron and nickel on the surface of the corrosion layer is detected. HCl is still able to penetrate the initial oxide layer of the metal and form metal chlorides. At 420°C the formation of NiCl₂ is thermodynamically possible as well, since ΔG for the reaction of nickel with HCl approaches negative values. FeCl₂ has a higher vapor pressure than NiCl₂ and evaporates faster. At 420°C the vapor pressure of CrCl₂ is almost zero. Thus, it remains largely in the corrosion layer. Due to the water gas shift reaction, H₂O can react with CrCl₂ to Cr₂O₃. At lower temperatures the equilibrium of the water gas shift reaction is shifted to the educts side, whereby less H₂O is produced. Thus, this subsequently leads to less Cr₂O₃ formation. NiCl₂ evaporates and diffuses to the

surface, where it forms nickel sulfide with H₂S of the gas phase.

At both temperatures and at high H₂S amounts, the ferritic material, K90941, showed an outward layer of iron sulfide and an inner layer, which contains chromium, besides iron and sulfur. Schulte et al. [19] found the same picture of corrosion and proposed that, for ferritic materials, first of all, formation and growth of a pore-free and gas tight sulfide layer takes place. Then the development of an inner layer occurs, in which the elements forming sulfides of higher stability than FeS in particular chromium are enriched. The scale on the austenitic material, N08811, differs from that of K90941 insofar as the outer FeS layer contains nickel. Additionally, the spinel phase FeCr₂S₄ was identified via XRD. Schulte et al. [19] suggested that this intermediate layer of FeCr₂S₄ is responsible for the lower sulfidation rate of the austenitic material compared to that of the ferritic steel. Thus, solid-state diffusion is slower and scale separation starts much later once a greater scale thickness is achieved. These mechanisms would fit with the findings of our experiments.

In the atmosphere with 200 ppm H₂S and at 580°C, the mass loss can mainly be attributed to the formation and sublimation of metal chlorides, which could be detected as FeCl₂ in the colder parts of the silica glass tube. When going to lower temperatures, the amount of detected FeCl₂ at the colder parts of the glass tube decreased. Still, chlorine could be detected by XRD and in the EDX mappings distributed over the whole corrosion product, with a higher incidence at the interface metal/corrosion layer and on top of the corrosion layer. This can be explained by the decreasing vapor pressure of the metal chlorides when going

to lower temperatures. Thus, the metal chlorides partly remain in the corrosion product.

At higher H₂S concentrations in the gas atmosphere and, thus, at higher sulfur vapor pressure, less chlorine could be detected in the EDX mappings compared to the findings at 200 ppm H₂S. Additionally, less metal chlorides could be detected at the colder parts of the tube even at high temperatures. EDX mappings also showed a smaller amount of oxygen in the corrosion products compared to the findings at 200 ppm H₂S. The reason for this might be the suppression of the water-gas shift reaction by H₂S [20, 21]. Since more H₂S diffuses through the corrosion layer, the water-gas shift reaction will not take place to the same extent as at lower H₂S contents in the gas atmosphere. XRD identified pure iron sulfide for K90941 and iron sulfide and FeCr₂S₄ in the case of N08811.

Two assumptions about the higher corrosion rate of the materials at higher H₂S contents are imaginable. The first assumption is that direct sulfidation of the materials takes place, where the mass loss is mainly attributed to the formation of sulfides. Due to the high lattice disorder of sulfides, as already known from literature [22, 23], the materials are not able to form protective scales and thus, continuous corrosion can take place. This would also fit with the findings of Schulte et al. [19].

The second assumption is that, first, chlorination of the materials takes place. Subsequently, sulfidation of the formed metal chlorides occurs. Thus, the higher corrosion rate is attributed to the formation of FeCl₂, which directly reacts with H₂S from the atmosphere. Thereby, HCl is released again, which can further react with the metal, thus accelerating the corrosion of the materials.

The effect of chlorine on the high temperature corrosion of alloys in sulfidizing atmospheres is still speculative. In general, the sulfidation rate is increased in the presence of hydrogen chloride, but a few results were published showing a decrease in corrosion rate [11]. Pan et al. [14] suggested that a reason for the prevention of sulfide growth of chromium containing steels in reducing atmospheres might be the fact that the outward diffusion of the metal chlorides in the scale slows down the penetration of H₂S, therefore limiting the possibility of formation of sulfides. Alternatively, HCl may be preferentially adsorbed on the surface of given oxides, partly inhibiting the reaction with H₂S. Yet, the influence of sulfur on the corrosion of the present commercial steels cannot be ignored because increasing the H₂S content in the given chlorine containing atmosphere leads to an acceleration of the corrosion for both materials. Thus, further research is necessary to verify the previous assumptions.

4. Conclusions

Commonly used construction materials like the ferritic steel K90941 and the austenitic steel N08811 were tested under conditions of a thermal cracking process of post-consumer plastics. The tests were performed at 420 °C and 580 °C for 72 h in gas atmospheres with varying H₂S content. The major conclusions obtained from this research are as follows:

1. The ferritic material showed a higher mass loss than the austenitic material under all conditions.
2. The mass loss resulted from either the sublimation of metal chlorides or the formation of iron sulfide.
3. In general, the mass loss increased with increasing H₂S content in the atmosphere and increasing temperature.
4. Corrosion products on the specimens showed a multi-layered structure, which differed depending on the conditions.
 - a. At 580 °C and 200 ppm H₂S, both materials showed the formation of a chromium oxide layer below a chromium sulfide layer, a depletion of iron and chromium and in the case of N08811 an enrichment of nickel at the border zone next to the corrosion products.
 - b. At 420 °C and 200 ppm H₂S, a layer of mixed iron-chromium sulfide was found for K90941, while N08811 showed a layer of mixed iron-nickel sulfides.
 - c. At higher H₂S amounts, the picture of corrosion did not change with temperature. The materials showed an outward layer of iron sulfide and an inner layer, which, besides iron and sulfur, contained chromium. The scale on N08811 differed from that on K90941 as the outer FeS layer contained nickel. In the corrosion products of N08811, the spinel FeCr₂S₄ was observed, which is attributed to be responsible for the lower sulfidation rate of this material compared to that of the ferritic steel.
5. Still, the temperature has a big influence on the mass loss of the materials, since higher temperatures accelerate the corrosion reactions. This is also true for the atmosphere with 200 ppm H₂S.

Summarizing, the austenitic material N08811 had better corrosion resistance under the tested conditions compared to the ferritic material K90941. Mixed gas atmospheres are challenging for a prediction of the high temperature corrosion behavior of alloys. In some studies, a reduction in the corrosion rate was found in these mixed gas atmospheres, but others showed an increase in corrosion. A thorough discussion of the obtained results is not possible at this moment. Further laboratory work in a range of simulated atmospheres of a pyrolysis process for post-consumer plastics and temperatures is required to obtain a detailed mechanism of corrosion in hydrogen chloride and hydrogen sulfide containing gas atmospheres.

Acknowledgements. The authors would like to thank OMV Downstream GmbH for the possibility to work on this project and the support from OMV E&P. The materials were provided by Sandvik and Schmidt + Clemens, which is gratefully acknowledged.

Funding. Open access funding provided by Montanuniversität Leoben.

Open Access This article is licensed under a Creative Commons Attribution 4.0 International License, which permits use, sharing, adaptation, distribution and reproduction in any medium or format, as long as you give appropriate credit to the original author(s) and the source, provide a link to the Creative Commons licence, and indicate if changes were made. The images or other third party material in this article are included in the article's Creative Commons licence, unless indicated otherwise in a credit line to the material. If material is not included in the article's Creative Commons licence and your intended use is not permitted by statutory

regulation or exceeds the permitted use, you will need to obtain permission directly from the copyright holder. To view a copy of this licence, visit <http://creativecommons.org/licenses/by/4.0/>.

References

- Schwalm, C.; Schütze, M.: The corrosion behavior of several heat resistant materials in air + 2vol.% Cl₂ at 300 to 800°C Part I—Fe base and Fe containing alloys, *Materials and Corrosion*, 51 (2000), pp 34–49
- Schmid, A.; Mori, G.; Haubner, R.; Weil, M.; Höning S.: Behaviour of S31400 and S32205 steels in HCl- and H₂S- containing gas atmospheres under a low oxygen partial pressure between 480 and 680°C, *Materials and Corrosion*, 69 (2018), pp 1–10
- Yu, J.; Sun, L.; Ma, C.; Qiao, Y.; Yao, H.: Thermal degradation of PVC: A review, *Waste Management*, 48 (2016), pp 300–314
- Zahs, A.; Spiegel, M.; Grabke, H.J.: The influence of alloying elements in the chlorine induced high temperature corrosion of Fe-Cr alloys in oxidizing atmospheres, *Materials and Corrosion*, 50 (1999), pp 561–578
- Bramhoff, D.; Grabke, H.J.; Schmidt, H.P.: The role of active elements in the oxidation behaviour of high temperature metals and alloys, *Petten, The Netherlands: Elsevier Science Publishers Ltd.*, 1989, pp 335–349
- Bakker, W.T.: The effect of chlorine on mixed oxidant corrosion of stainless steel, *Materials at high temperatures*, 14 (1997), pp 197–206
- Lee, S.H.; Castaldi, M.J.: The effects of varied hydrogen chloride gas concentrations on corrosion rates of commercial tube alloys under simulated environment of WTE facilities, *NAWTEC16 16th Annual North American Waste-to-Energy Conference*, Philadelphia, Pennsylvania, USA, 2008, paper no. 1916
- Prescott, R.; Stott, F.H.; Elliott, P.: The degradation of metals in a hydrogen chloride containing gas at high temperature, *Corrosion Science*, 29 (1989), pp 465–475
- Bramhoff, D.; Grabke, H.J.; Reese, E.: Influence of HCl and Cl₂ on high temperature corrosion of 2 ¼ Cr1Mo steel in atmospheres with high oxygen pressures, *Werkstoffe und Korrosion*, 41 (1990), pp 303–307
- Bramhoff, D.; Grabke, H.J.; Schmidt, H.P.: Influence of HCl and N₂ on high temperature corrosion in atmospheres with low oxygen pressures, *Werkstoffe und Korrosion*, 40 (1989), pp 642–650
- Haanappel, V.A.C.; Fransen, T.; Gellings, P.J.: Chlorine-induced high temperature corrosion: I. Metals and Alloys—A review, *High Temperature Materials and Processes*, 10 (1992), pp 67–89
- Asteman, H.; Spiegel, M.: Investigation of the HCl (g) attack on pre-oxidized pure Fe, Cr, Ni and commercial 304 steel at 400°C, *Corrosion Science*, 49 (2007), pp 3626–3637
- Schmid, A.; Mori, G.; Strobl, S.; Haubner, R.; Höning, S.: Corrosion of various Fe and Ni based alloys in HCl, H₂S containing environments, with low oxygen partial pressure, at 680°C, Presentation: EUROCORR 2017, 20th International Corrosion Congress & Process Safety Congress 2017, Prague, Czech Republic, 03.09.–07.09.2017; in Conference Proceedings EUROCORR 2017, 2017, Paper-Nr. 79016, 10
- Pan, T.J.; Gesmundo, F.; Niu, Y.: Corrosion behaviour of three iron-based alloy in reducing atmospheres containing HCl and H₂S at 600°C, *Corrosion Science*, 49 (2007), pp 1362–1377
- Bakker, W.T.; Perkins, R.A.: Beyond mixed oxidant corrosion-corrosion phenomena in gasifiers, EPRI Gasification Conference, 1990
- Bakker, W.T.; Perkins, R.A.: Materials for coal gasification, ASM International, Bakker, W.T.; Dapkunas, S.; Hill, V. (Eds.), 1988, pp. 85–96
- Schmid, A.; Mori, G.; Bucher, E.; Haubner, R.: Model about the course of corrosion reactions of austenitic steels in H₂S-, HCl- and CO₂-containing atmospheres at 680°C, *Oxidation of Metals*, 91 (2019), pp 1–10
- Kunze, E.; *Korrosion und Korrosionsschutz*, Weinheim, Deutschland: Wiley-VCH Verlag GmbH, 2001
- Schulte, M.; Rahmel, A.; Schütze, M.: The Sulfidation Behavior of Several Commercial Ferritic and Austenitic Steels, *Oxidation of Metals*, 49 (1998), pp 33–70
- Ruppi, S.; Larsson, A.: Chemical vapour deposition of κ-Al₂O₃, *Thin Solid Films*, 388 (2001), pp 50–61
- Blomqvist, A.; Århammar, C.; Pedersen, H.; Silvearv, F.; Norgren, S.; Ahuja, R.: Understanding the catalytic effects of H₂S on CVD-growth of alpha-alumina: Thermodynamic gas-phase simulations and density functional theory, *Surface and Coatings Technology*, 206 (2011), pp 1771–1779
- Young, D.J.: *High Temperature Oxidation and Corrosion of Metals*, Amsterdam, The Netherlands: Elsevier, 2016
- Khanna, A.: *High Temperature Corrosion*, World Scientific, 2016, pp 1–31

Publisher's Note. Springer Nature remains neutral with regard to jurisdictional claims in published maps and institutional affiliations.